


Propagating Ferrodark Solitons in a Superfluid: Exact Solutions and Anomalous Dynamics

Xiaoquan Yu^{1,2,*} and P. B. Blakie²¹Graduate School of China Academy of Engineering Physics, Beijing 100193, China²Department of Physics, Centre for Quantum Science, and Dodd-Walls Centre for Photonic and Quantum Technologies, University of Otago, Dunedin 9016, New Zealand
 (Received 27 April 2021; revised 26 July 2021; accepted 1 February 2022; published 24 March 2022)

Exact propagating topological solitons are found in the easy-plane phase of ferromagnetic spin-1 Bose-Einstein condensates, manifesting themselves as kinks in the transverse magnetization. Propagation is only possible when the symmetry-breaking longitudinal magnetic field is applied. Such solitons have two types: a low energy branch with positive inertial mass and a higher energy branch with negative inertial mass. Both types become identical at the maximum speed, a new speed bound that is different from speed limits set by the elementary excitations. The physical mass, which accounts for the number density dip, is negative for both types. In a finite one-dimensional system subject to a linear potential, the soliton undergoes oscillations caused by transitions between the two types occurring at the maximum speed.

DOI: [10.1103/PhysRevLett.128.125301](https://doi.org/10.1103/PhysRevLett.128.125301)

Introduction.—The inertial mass (or effective mass) of emergent quasiparticles contains rich information on the dynamics of quantum many body systems [1]. In quantum fluids the inertial mass of a topological soliton is determined by both the kinetic and interaction energies and is a key quantity governing its dynamics. For instance, the one-dimensional (1D) motion of a dark or gray soliton in a superfluid (bosonic or fermionic) can be described by a Newton equation with negative inertial mass [2], leading to oscillations in a harmonic trap [2–4]. The sign of inertial mass also signals the stability of the soliton in a system of higher than one spatial dimension. Indeed, two- or three-dimensional solitons with negative inertial mass typically decay [5] due to the snake instability (growth of transverse deformations) [6–8]. It is a rather general feature for solitons in quantum fluids that the soliton energy decreases with increasing velocity, giving rise to a negative inertial mass. Relevant examples are dark or gray solitons in bosonic and fermionic quantum gases [2], phase domain walls in binary Bose-Einstein condensates (BECs) with strong coherent coupling [9–12], magnetic solitons in both binary [15] and antiferromagnetic spin-1 BECs [16,17]. A soliton with positive inertial mass should be stable in higher dimensions and exhibit anomalous dynamics.

In this Letter we report on the discovery of two types of exact topological solitons that have positive and negative inertial mass, respectively, occurring as kinks in the transverse magnetization of a ferromagnetic spin-1 BEC. We refer to them as ferrodark solitons (FDSs). In the zero velocity limit the FDSs connect to the stationary magnetic domain walls (MDWs) recently found in Ref. [18]. The FDSs can only propagate at a finite speed in a longitudinal magnetic field which provides a necessary condition for the

motion, i.e., breaking the transverse magnetization conservation. In addition, the FDSs exhibit a number of other novel features different from conventional solitons. When traveling, the transverse magnetization is always zero in the core of a FDS and hence there is no magnetic current. The motion arises from a coupling between the magnetization and nematic degrees of freedom caused by the magnetic field. Interestingly, the moving speed is not limited by group velocities of elementary excitations but has a new speed bound, at which the two types of solitons become identical. We study dynamics of the soliton in a hard-wall trapped quasi-1D system with a superimposed linear potential and find transitions between the two types via internal spin currents, leading to an oscillatory motion. While we focus on the exactly solvable case, FDSs exist with the characteristic features revealed by the exact solutions in the whole easy-plane phase.

Spin-1 BECs.—The Hamiltonian density of a spin-1 condensate reads

$$\mathcal{H} = \frac{\hbar^2 |\nabla \psi|^2}{2M} + \frac{g_n}{2} |\psi^\dagger \psi|^2 + \frac{g_s}{2} |\psi^\dagger \mathbf{S} \psi|^2 + q \psi^\dagger S_z^2 \psi, \quad (1)$$

where the three-component wave function $\psi = (\psi_{+1}, \psi_0, \psi_{-1})^T$ describes the atomic hyperfine state $|F=1, m=+1, 0, -1\rangle$, M is the atomic mass, $g_n > 0$ is the density interaction strength, g_s is the spin-dependent interaction strength, $\mathbf{S} = (S_x, S_y, S_z)$ with $S_{j=x,y,z}$ being the spin-1 matrices [19], and q denotes the quadratic Zeeman energy. The spin-dependent interaction term allows for spin-mixing collisions between $m=0$ and $m=\pm 1$ atoms. At the mean-field level, the dynamics of the field ψ is governed by the Gross-Pitaevskii equations (GPEs)

$$i\hbar \frac{\partial \psi_{\pm 1}}{\partial t} = [H_0 + g_s(n_0 + n_{\pm 1} - n_{\mp 1}) + q]\psi_{\pm 1} + g_s \psi_0^2 \psi_{\mp 1}^*,$$

$$i\hbar \frac{\partial \psi_0}{\partial t} = [H_0 + g_s(n_{+1} + n_{-1})]\psi_0 + 2g_s \psi_0^* \psi_{+1} \psi_{-1}, \quad (2)$$

where $H_0 = -\hbar^2 \nabla^2 / 2M + g_n n$, $n_m = |\psi_m|^2$ and $n = \sum n_m$. Spin-1 BECs support magnetic order [20–24], quantified by the order parameter magnetization $\mathbf{F} \equiv \psi^\dagger \mathbf{S} \psi$. This identifies ferromagnetic order $|\mathbf{F}| > 0$ for $g_s < 0$ (^{87}Rb , ^7Li) and antiferromagnetic order $\mathbf{F} = 0$ for $g_s > 0$ (^{23}Na).

Quadratic Zeeman driven propagating FDSs.—We consider a uniform ferromagnetic ($g_s < 0$) spin-1 BEC with total number density n_b . In the presence of a uniform magnetic field along the z axis ($0 < q < -2g_s n_b$) [25], the uniform ground state with zero longitudinal magnetization ($F_z = n_{+1}^b - n_{-1}^b = 0$) is transversally magnetized (easy-plane phase) [23,24], characterized by the transverse magnetization $F_\perp \equiv F_x + iF_y = \sqrt{8n_{\pm 1}^b n_0^b} e^{i\tau}$, where $n_{\pm 1}^b = (1 - \tilde{q})n_b/4$ and $n_0^b = n_b(1 + \tilde{q})/2$ are the component densities, and $\tilde{q} \equiv -q/(2g_s n_b)$. The SO(3) symmetry is broken by the magnetic field and the system processes the remnant SO(2) symmetry, parametrized by the rotational angle about the z axis τ .

In the following we focus on a 1D system. In the easy plane phase, exact transverse magnetic kink solutions of Eq. (2) are found for a large spin-dependent interaction strength $g_s = -g_n/2$ and $0 < q < -2g_s n_b$. There are two types of such traveling kinks and the transverse magnetizations and the total number densities read

$$F_\perp^{\text{I,II}}(x, t) = -e^{i\tau} \sqrt{n_b^2 - \frac{q^2}{g_n^2}} \tanh\left(\frac{x - Vt}{\ell^{\text{I,II}}}\right), \quad (3)$$

$$n^{\text{I,II}}(x, t) = n_b - \frac{g_n n_b - MV^2 \mp Q}{2g_n} \text{sech}^2\left(\frac{x - Vt}{\ell^{\text{I,II}}}\right), \quad (4)$$

where V is the moving velocity,

$$\ell^{\text{I,II}} = \sqrt{\frac{2\hbar^2}{M(g_n n_b - MV^2 \mp Q)}}, \quad (5)$$

and

$$Q = \sqrt{M^2 V^4 + q^2 - 2g_n M n_b V^2}. \quad (6)$$

The above kink solutions are of Ising-type and connect regions transversely magnetized in opposite directions [26]. Hereafter we refer to them as ferrodark solitons and the minus (plus) sign in front of Q specifies type-I (II) FDS. Unless specified, we choose $\tau = 0$ for convenience. Note that at the core $x = Vt$, $F_\perp^{\text{I,II}} = 0$ while $n^{\text{I,II}} \neq 0$.

The corresponding wave functions at the exactly solvable region are shown in Table I. Recently a ^7Li spin-1 BEC has been prepared in the strong spin interacting regime close to the exactly solvable point [27].

The inequality $Q^2 \geq 0$ gives rise to the upper bound of the traveling speed [30]

$$V \leq \sqrt{\frac{g_n n_b}{M}} \sqrt{1 - \sqrt{1 - \left(\frac{q}{g_n n_b}\right)^2}} \equiv c_{\text{FDS}}. \quad (7)$$

The speed bound Eq. (7) is markedly different from the group velocities of low-lying elementary excitations which normally set the speed limits [31]. In the easy-plane phase, the gap-less branches of the elementary excitations involve spin waves of magnetization \mathbf{F} (dominantly) and mixed waves of F_\perp and n , with group velocities at long wavelengths $c_m = \sqrt{q/(2M)}$ and $c_{\text{mp}} = \sqrt{n_b(g_n + g_s)}/M$, respectively [32]. Strikingly, for $1 > q/g_n n_b > \sqrt{3}/2$, $c_{\text{FDS}} > c_{\text{mp}} > c_m$, implying that the FDSs can travel with speed greater than c_m and c_{mp} . This can happen because a propagating FDS does not involve magnetic currents (see below). Another conspicuous feature is that the soliton profile does not vanish at $V = c_{\text{FDS}}$ (see Fig. 1). The velocity of gray solitons in scalar BECs is bounded by the speed of sound, and at this velocity the soliton disappears [31]. At the transition point $q = g_n n_b$, the easy-plane phase becomes unstable, signaled by the divergence of ℓ^{I} .

Similar to scalar gray solitons, the density dip of the type-II FDS becomes shallower for greater velocities [Fig. 1(d)]. In contrast, for the type-I FDS the density

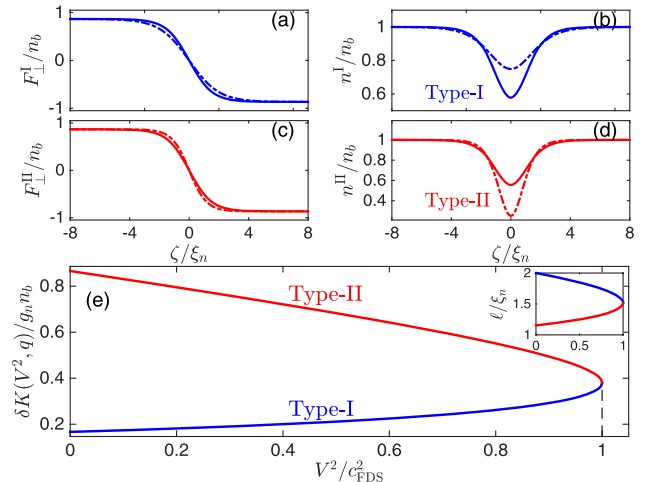


FIG. 1. (a)–(d) Transverse magnetizations and densities of FDSs at $g_s = -g_n/2$ and $\tilde{q} = 0.5$ for different velocities: $V/c_{\text{FDS}} = 1$ (solid line); $V/c_{\text{FDS}} = 0.1$ (dashed line). (e) Excitation energies of FDSs as functions of V^2 evaluated from Eqs. (10) and (12) at $\tilde{q} = 0.5$. Here $\zeta = x - Vt$. The inset shows widths of FDSs, where the x axis is the same as in (e).

dip behaves anomalously and deepens with increasing velocity [Fig. 1(b)]. Crucially, at the maximum velocity $V = c_{\text{FDS}}$, $Q = 0$ and the two types of FDSs become identical upon a U(1) gauge transformation, namely, $\psi^I(x, t) = i\psi^{\text{II}}(x, t)$ (see Table I).

When $q \rightarrow 0$, $c_{\text{FDS}} \rightarrow 0$, implying that the propagation is prohibited in the absence of a magnetic field, where the conservation law of magnetization is restored. In this limit, the two types become degenerate and are related via a SO(3) spin rotation [18]. Clearly, a magnetic field does not automatically induce motion. At $V = 0$ the FDSs recover stationary MDWs at finite q [18,33].

Currents.—Moving FDSs involve nematic degrees of freedom and internal spin currents. Since the magnetization is zero at the core of a moving FDS, there is no magnetic current, i.e., $\mathbf{J}_i^f \equiv \hbar/(2Mi)(\psi^\dagger S_i \nabla \psi - \text{H.c.}) = 0$. According to the continuity equation

$$\frac{\partial F_i}{\partial t} + \nabla \cdot \mathbf{J}_i^f = K_{iz}, \quad (8)$$

the time evolution of magnetic domains enclosed by the FDSs is governed by the source term $K_{iz} = (2q/\hbar)\hat{K}_{iz}$ [35,36], where $\hat{K}_{iz} = \sum_k \epsilon_{izk} N_{zk}$, $N_{ij} = \psi^\dagger \hat{N}_{ij} \psi$ is the nematic tensor, $\hat{N}_{ij} = (S_i S_j + S_j S_i)/2$ and $i, j \in \{x, y, z\}$. For propagating FDSs $\hat{K}_{iz} \neq 0$ and $\hat{K}_{iz} \rightarrow 0$ as $V \rightarrow 0$. At $q = 0$, $K_{iz} = 0$, and FDSs must stay still.

The continuity equations for particle number in each spin state read $\partial n_{\pm 1}/\partial t + \nabla \cdot \mathbf{J}_{\pm 1} + J_{\pm 1 \rightarrow 0} = 0$, and $\partial n_0/\partial t + \nabla \cdot \mathbf{J}_0 + \sum_{m=-1,+1} J_{0 \rightarrow m} = 0$, where

$\mathbf{J}_{\pm 1,0} = \hbar/(2Mi)(\psi_{\pm 1,0}^* \nabla \psi_{\pm 1,0} - \text{H.c.})$ are the component number current densities [37], and

$$J_{\pm 1 \rightarrow 0} = -J_{0 \rightarrow \pm 1} = \frac{g_s}{\hbar i} [(\psi_0^*)^2 \psi_{-1} \psi_{+1} - \text{H.c.}] \quad (9)$$

are the internal spin currents, reflecting the internal coherent spin exchange dynamics: $|00\rangle \leftrightarrow | +1\rangle - | -1\rangle$ [20–22]. Rewriting Eq. (9) in terms of wave function phases $(\theta_{\pm 1,0})$ and densities, we obtain $J_{\pm 1 \rightarrow 0} = (2n_0 n_{\pm 1} g_s / \hbar) \times \sin[2(\theta_{\pm 1} - \theta_0)]$ which suggests an analogy to Josephson currents [38,39]. It is important to note that these built-in currents are invariant under SO(2) rotations ($e^{-i\tau S_z}$). Table I shows the expressions of currents at the exactly solvable point.

Excitation energy and inertial mass.—The excitation energy of FDSs can be obtained by evaluating the difference of grand canonical energies $\delta K = K_{\text{FDS}} - K_g$, where $K_{\text{FDS}} = \int dx (\mathcal{H}[\psi] - \mu n)$, $K_g = \int dx (\mathcal{H}[\psi_g] - \mu n_b)$, ψ_g is the ground state wave function, and $\mu = (g_n + g_s)n_b + q/2$ is the chemical potential. For type-I FDSs, we obtain

$$\delta K^1(q, V^2) = \frac{\sqrt{2}\hbar(g_n n_b - MV^2 - Q)^{3/2}}{3g_n \sqrt{M}}. \quad (10)$$

Expanding Eq. (10) around $V = 0$, we have $\delta K^1(q, V^2) = \delta K^1(q, 0) + M_{\text{in}}^1 V^2/2 + o(V^2)$, where $\delta K^1(q, 0) = \sqrt{2}\hbar(g_n n_b - q)^{3/2}/(3g_n \sqrt{M})$ and the inertial mass is

TABLE I. Wave functions and currents of propagating FDSs in the exactly solvable regime ($g_s = -g_n/2$, $0 < q < -2g_s n_b$). The coefficients satisfy the following relations: $\kappa^{\text{I,II}} \alpha^{\text{I,II}} = \delta^{\text{I,II}} \beta^{\text{I,II}}$ and $(\alpha^{\text{I,II}})^2 + (\delta^{\text{I,II}})^2 = (\beta^{\text{I,II}})^2 + (\kappa^{\text{I,II}})^2 = 1$. It is straightforward to check that stationary solutions are obtained when $V \rightarrow 0$ [18,28]. Here $\zeta = x - Vt$ and $\mathcal{K}^2 \equiv \sum_i K_{iz}^2$ is SO(2) rotationally invariant [29]. The counter-propagating solution is $\psi^*(x, -t)$. Interestingly, $J_{\pm 1}^x$ and J_0^x have opposite signs and $\int dx J_{\pm 1 \rightarrow 0} = 0$, forming a Josephson vortexlike structure near the core of a FDS.

	Type-I	Type-II
ψ	$\psi_{\pm 1}^{\text{I}}(x, t) = \sqrt{n_b^{\pm 1}}[\alpha^{\text{I}} \tanh(\zeta/\ell^{\text{I}}) + i\delta^{\text{I}}]$ $\psi_0^{\text{I}}(x, t) = \sqrt{n_b^0}[\beta^{\text{I}} + i\kappa^{\text{I}} \tanh(\zeta/\ell^{\text{I}})]$ $\alpha^{\text{I}} = -\sqrt{MV^2(g_n n_b + q)/q(q + MV^2 - Q)}$ $\delta^{\text{I}} = \sqrt{(q - MV^2 - Q)/2q}$ $\beta^{\text{I}} = \sqrt{(q + MV^2 + Q)/2q}$ $\kappa^{\text{I}} = -\sqrt{[q(q - Q) - g_n M n_b V^2]/q(q + MV^2 - Q)}$	$\psi_{\pm 1}^{\text{II}} = \sqrt{n_b^{\pm 1}}[\beta^{\text{II}} + i\kappa^{\text{II}} \tanh(\zeta/\ell^{\text{II}})]$ $\psi_0^{\text{II}} = \sqrt{n_b^0}[\alpha^{\text{II}} \tanh(\zeta/\ell^{\text{II}}) + i\delta^{\text{II}}]$ $\alpha^{\text{II}} = -\sqrt{MV^2 + q - Q}(q - MV^2 + Q)/2\sqrt{qMV^2(g_n n_b - MV^2 + Q)}$ $\delta^{\text{II}} = -\sqrt{(q + MV^2 - Q)/2q}$ $\beta^{\text{II}} = \sqrt{(q - MV^2 + Q)/2q}$ $\kappa^{\text{II}} = (q + MV^2 - Q)\sqrt{q - MV^2 + Q}/2\sqrt{qMV^2(g_n n_b - MV^2 + Q)}$
\mathcal{K}	$(2\sqrt{2}q\sqrt{n_b^{\pm 1} n_b^0} \delta^{\text{I}} \beta^{\text{I}} / \hbar) \text{sech}^2(\zeta/\ell^{\text{I}})$	$(2\sqrt{2}q\sqrt{n_b^0 n_b^{\pm 1}} \delta^{\text{II}} \beta^{\text{II}} / \hbar) \text{sech}^2(\zeta/\ell^{\text{II}})$
$J_{\pm 1}^x$	$-(n_b^{\pm 1} \alpha^{\text{I}} \delta^{\text{I}} \hbar / \ell^{\text{I}} M) \text{sech}^2(\zeta/\ell^{\text{I}})$	$(n_b^{\pm 1} \kappa^{\text{II}} \beta^{\text{II}} \hbar / \ell^{\text{II}} M) \text{sech}^2(\zeta/\ell^{\text{II}})$
J_0^x	$(n_b^0 \kappa^{\text{I}} \beta^{\text{I}} \hbar / \ell^{\text{I}} M) \text{sech}^2(\zeta/\ell^{\text{I}})$	$-(n_b^0 \alpha^{\text{II}} \delta^{\text{II}} \hbar / \ell^{\text{II}} M) \text{sech}^2(\zeta/\ell^{\text{II}})$
$J_{\pm 1 \rightarrow 0}$	$-[4g_s(\delta^{\text{I}} \kappa^{\text{I}} + \beta^{\text{I}} \alpha^{\text{I}}) \delta^{\text{I}} \beta^{\text{I}} n_b^{\pm 1} n_b^0 / \hbar] \times \tanh(\zeta/\ell^{\text{I}}) \text{sech}^2(\zeta/\ell^{\text{I}})$	$[4g_s(\kappa^{\text{II}} \delta^{\text{II}} + \beta^{\text{II}} \alpha^{\text{II}}) \delta^{\text{II}} \beta^{\text{II}} n_b^{\pm 1} n_b^0 / \hbar] \times \tanh(\zeta/\ell^{\text{II}}) \text{sech}^2(\zeta/\ell^{\text{II}})$

$$M_{\text{in}}^{\text{I}} \equiv 2 \left. \frac{\partial \delta K^{\text{I}}}{\partial V^2} \right|_{V=0} = \frac{\sqrt{2M\hbar}(g_n n_b - q)^{3/2}}{g_n q} > 0. \quad (11)$$

As $q \rightarrow 0$, $M_{\text{in}}^{\text{I}} \rightarrow +\infty$ and the FDS becomes infinitely heavy, consistent with the absence of propagation at zero magnetic field due to the conservation of magnetization [18]. In contrast to the normal behavior of gray solitons, the excitation energy (δK^{I}) of the type-I FDS increases monotonically with increasing V^2 [Fig. 1(e)], in accordance with the anomalous behavior of the density [Fig. 1(b)]. It is worth noting that here every component density has a dip (see Table I) and the inertial mass of type-I FDSs being positive is a highly nontrivial nonlinear effect. Following conventional arguments [5] the positive inertial mass explains the stability of MDWs against transverse snake perturbations in two dimensions [18].

The physical mass is defined as $M_{\text{phy}} \equiv M\delta N$, where $\delta N = \int dx[n(x) - n_b]$. For type-I FDSs, we obtain $M_{\text{phy}}^{\text{I}} = -2\hbar^2/(g_n \ell^{\text{I}}) < 0$. In the presence of an external potential U , a soliton with negative physical mass experiences an effective force from the surrounding liquid pointing in the opposite direction to $-\nabla U$ (similar to buoyant force). For a scalar gray soliton the inertial and the physical masses are both negative and it exhibits normal particlelike behavior, e.g., oscillations in a harmonic potential [2,3]. Whereas a type-I FDS in a harmonic potential would be expelled, i.e., moves away from the potential minimum.

The excitation energy of the type-II FDS is

$$\delta K^{\text{II}}(q, V^2) = \frac{\sqrt{2\hbar}(g_n n_b - MV^2 + Q)^{3/2}}{3g_n \sqrt{M}} \quad (12)$$

with $\partial \delta K^{\text{II}}/\partial V^2 < 0$ [Fig. 1(e)]. Expansion of Eq. (12) leads to $\delta K^{\text{II}}(q, V^2) = \delta K^{\text{II}}(q, 0) + M_{\text{in}}^{\text{II}} V^2/2 + o(V^2)$, where $\delta K^{\text{II}}(q, 0) = \sqrt{2\hbar}(g_n n_b + q)^{3/2}/(3g_n \sqrt{M})$ and the inertial mass

$$M_{\text{in}}^{\text{II}} \equiv 2 \left. \frac{\partial \delta K^{\text{II}}}{\partial V^2} \right|_{V=0} = -\frac{\sqrt{2M\hbar}(g_n n_b + q)^{3/2}}{g_n q} < 0. \quad (13)$$

Consistently, $M_{\text{in}}^{\text{II}} \rightarrow -M_{\text{in}}^{\text{I}} \rightarrow -\infty$ as $q \rightarrow 0$. The physical mass $M_{\text{phy}}^{\text{II}} = -2\hbar^2/(g_n \ell^{\text{II}}) < 0$. Thus, the inertial and physical mass of the type-II FDS is similar to those of ordinary gray or dark solitons. Excitation energies of type-I and type-II FDSs coincide smoothly at the maximum speed [Fig. 1(e)], making transitions between the two types of FDSs possible under certain circumstances.

Oscillations between type-I and type-II FDSs.—As discussed earlier the FDS does not vanish as $V \rightarrow c_{\text{FDS}}$, so a natural question is what will happen if it is further accelerated? Let us consider a hard-wall trapped quasi-1D spin-1 BEC subjected to a linear potential whose gradient is along the positive x axis. A $V = 0$ type-I FDS is initially placed near the left end of the system, and the later dynamic

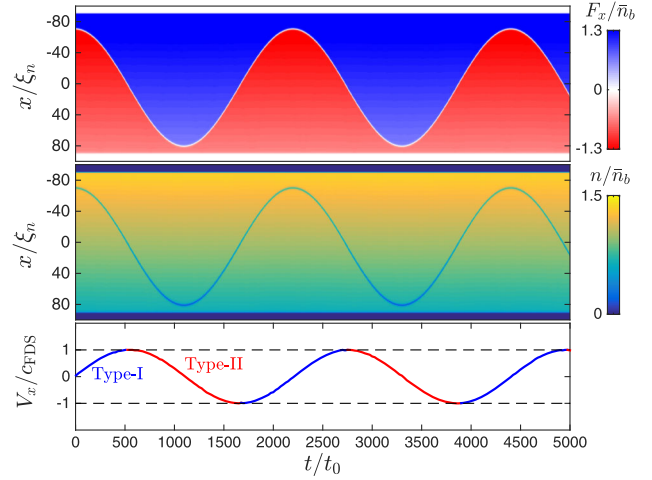


FIG. 2. Oscillations of a FDS in a hard-wall trapped spin-1 BEC with a superimposed linear potential [41]. The system size is $200\xi_n$, $g_s/g_n = -1/2$ and $\tilde{q} = q/(-2g_s \bar{n}_b) = 0.3$. Here \bar{n}_b is the average density, $t_0 = \hbar/g_n \bar{n}_b$ and $\xi_n = \hbar/\sqrt{Mg_n \bar{n}_b}$ is the density healing length. Upper and middle panels show spin and density dynamics of a FDS, respectively. The transverse magnetization is always zero at the core (see also Fig. S3 [32]) and the topological characteristic, i.e., the sign change of F_x is kept. Bottom panel shows the velocity of the FDS as a function of time, obtained by taking the derivative of its position with respect to time. The slope refers to the acceleration of the FDS and indicates the sign of the inertial mass (positive: blue; negative: red). The transition between type-I and type-II FDSs occurs when the slope changes sign at the maximum speed. Here c_{FDS} is the local speed limit for the (background) density at the position where dV_x/dt changes sign.

shows, surprisingly, a periodic motion. The FDS accelerates until it reaches the maximum speed (the local value of c_{FDS} [40]) at which point it smoothly transforms into a type-II FDS. Because of the sign change of the inertial mass (or more generally $\partial \delta K^{\text{I}}/\partial V^2 > 0 \rightarrow \partial \delta K^{\text{II}}/\partial V^2 < 0$), it starts to accelerate in the opposite direction. After reaching the turning point, the FDS starts to move to the left. It converts back to the type-I FDS and experiences positive acceleration again when gaining the maximum speed. Later it returns to the initial configuration. Note that during the motion there is no sign change of the physical mass. Numerical simulations show that this process continues without decay (see Fig. 2 and a movie in the Supplemental Material [32]).

During the motion the total number density profile of the soliton has only minor changes with respect to the local background density (see Fig. 2, and Fig. S3 [32]). However, internal oscillations (driven by the gradient of the external potential) between $m = \pm 1$ and $m = 0$ spin states near the core take place though the internal currents $J_{\pm 1 \leftrightarrow 0}$ (Fig. 3, and Fig. S4 [32]), inducing transitions between type-I and type-II FDSs. Accounting for the varying density and the potential energy, we map the FDS energy δK extracted from the simulation to its corresponding values

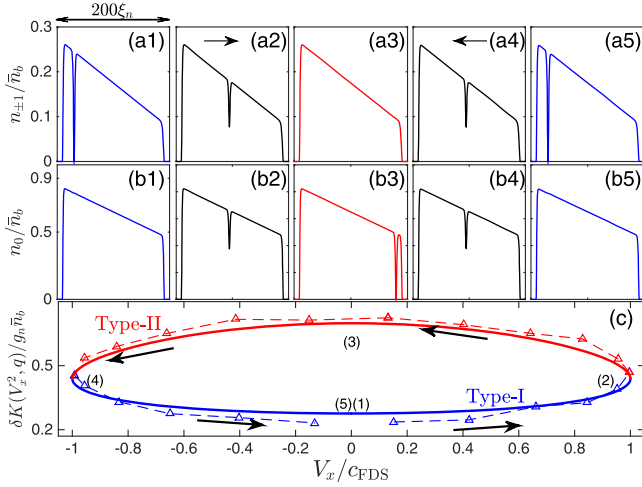


FIG. 3. Internal oscillations between $m = \pm 1$ and $m = 0$ spin states and the excitation energy for one complete cycle of the motion described in Fig. 2. The black arrows specify the evolution direction. (a1)–(b5) show component densities of the initial state (type-I FDS with zero velocity) [blue], at the maximum velocity [black], at the turning point (type-II FDS with zero velocity) [red], at the negative maximum speed [black], and of the final state (returning the initial state) [blue], respectively. (c) shows analytical predictions (solid lines) for $n_b = \bar{n}_b$ vs numerical results (markers) for the mapped uniform system with the same density (see main text). Number labels indicate the stages corresponding to those showing in the upper panels. Note that the total energy [43] is conserved.

for a uniform system [32], and find that it oscillates between lower branch (type-I) and higher branch (type-II) [Fig. 3(c)], as predicted [42].

It should be emphasized that away from the exact solvable parameter region ($g_s = -g_n/2$, $0 < q < -2g_s n_b$) the characteristic features of the oscillating dynamics hold in general (Fig. S5 [32]). Such an oscillation is a nonlinear phenomenon and is a result of a combination of internal spin currents induced by spin-dependent interactions, the external potential and two types of solitons being smoothly connected at the maximum speed. It occurs in a system without built-in periodicity and is distinct from the celebrated phenomenon of Bloch oscillations where the key ingredient is the presence of a band structure.

Conclusion.—We discover a propagating magnetic kink corresponding to a topological soliton with negative physical mass and positive inertial mass in the easy-plane phase of a ferromagnetic spin-1 BEC. It can convert to its higher energy counterpart with negative physical and inertial mass at a novel maximum speed that can be greater than the group velocities of elementary excitations which normally set the speed limits. The transition between the two types induces oscillations in a linear potential [44]. Our findings could be relevant to out-of-equilibrium quench dynamics in 1D ferromagnetic superfluids [46,47]. Investigations of ferrodark solitons are also within the scope of current spin-1 BEC experiments [48–52].

We thank M. Antonio, L. Qiao, D. Baillie, and Y. Yang for useful discussions. We particularly thank J.N. BiGuo for pointing out that the energy expression of type-I FDSs can be simplified to the current form. X. Y. acknowledges support from NSAF (No. U1930403) and NSFC (No. 12175215). P. B. B acknowledges support from the Marsden Fund of the Royal Society of New Zealand.

*xqyu@g scaep.ac.cn

- [1] G. D. Mahan, *Many-Particle Physics* (Springer Science & Business Media, New York, 2013).
- [2] R. G. Scott, F. Dalfovo, L. P. Pitaevskii, and S. Stringari, *Phys. Rev. Lett.* **106**, 185301 (2011).
- [3] V. V. Konotop and L. Pitaevskii, *Phys. Rev. Lett.* **93**, 240403 (2004).
- [4] T. Busch and J. R. Anglin, *Phys. Rev. Lett.* **84**, 2298 (2000).
- [5] A. M. Kamchatnov and L. P. Pitaevskii, *Phys. Rev. Lett.* **100**, 160402 (2008).
- [6] E. Kuznetsov and S. Turitsyn, *Zh. Eksp. Teor. Fiz.* **94**, 129 (1988).
- [7] A. E. Muryshev, H. B. van Linden van den Heuvell, and G. V. Shlyapnikov, *Phys. Rev. A* **60**, R2665 (1999).
- [8] Long wavelength transverse deformations of a soliton with negative inertial mass will be enhanced and eventually lead to a breakdown of a soliton.
- [9] A. Gallemí, L. P. Pitaevskii, S. Stringari, and A. Recati, *Phys. Rev. A* **100**, 023607 (2019).
- [10] C. Qu, M. Tylutki, S. Stringari, and L. P. Pitaevskii, *Phys. Rev. A* **95**, 033614 (2017).
- [11] S. S. Shamilov and J. Brand, *SciPost Phys.* **4**, 18 (2018).
- [12] In coherently coupled BECs, the Son-Stephanov phase domain wall [13] has positive inertial mass for weak coherent coupling strengths [9–11]. However a long wall fragments into smaller ones due to the bending caused by vortices on the ends of the wall [9,14].
- [13] D. T. Son and M. A. Stephanov, *Phys. Rev. A* **65**, 063621 (2002).
- [14] K. Ihara and K. Kasamatsu, *Phys. Rev. A* **100**, 013630 (2019).
- [15] C. Qu, L. P. Pitaevskii, and S. Stringari, *Phys. Rev. Lett.* **116**, 160402 (2016).
- [16] A. Farolfi, D. Trypogeorgos, C. Mordini, G. Lamporesi, and G. Ferrari, *Phys. Rev. Lett.* **125**, 030401 (2020).
- [17] X. Chai, D. Lao, K. Fujimoto, R. Hamazaki, M. Ueda, and C. Raman, *Phys. Rev. Lett.* **125**, 030402 (2020).
- [18] X. Yu and P. B. Blakie, *Phys. Rev. Research* **3**, 023043 (2021).
- [19] Generators of the rotational group SO(3):

$$S_x = \frac{1}{\sqrt{2}} \begin{pmatrix} 0 & 1 & 0 \\ 1 & 0 & 1 \\ 0 & 1 & 0 \end{pmatrix}, \quad S_y = \frac{i}{\sqrt{2}} \begin{pmatrix} 0 & -1 & 0 \\ 1 & 0 & -1 \\ 0 & 1 & 0 \end{pmatrix},$$

$$S_z = \begin{pmatrix} 1 & 0 & 0 \\ 0 & 0 & 0 \\ 0 & 0 & -1 \end{pmatrix}.$$

- [20] T.-L. Ho, *Phys. Rev. Lett.* **81**, 742 (1998).
- [21] T. Ohmi and K. Machida, *J. Phys. Soc. Jpn.* **67**, 1822 (1998).
- [22] L. E. Sadler, J. M. Higbie, S. R. Leslie, M. Vengalattore, and D. M. Stamper-Kurn, *Nature (London)* **443**, 312 (2006).
- [23] D. M. Stamper-Kurn and M. Ueda, *Rev. Mod. Phys.* **85**, 1191 (2013).
- [24] Y. Kawaguchi and M. Ueda, *Phys. Rep.* **520**, 253 (2012), spinor Bose–Einstein condensates.
- [25] In experiments, the quadratic Zeeman term is a combination of contributions from a magnetic field and a microwave [23,24].
- [26] Note that they are topological excitations in a uniform stable ground state but not interfaces between regions in a fragmented state.
- [27] S. J. Huh, K. Kim, K. Kwon, and J.-y. Choi, *Phys. Rev. Research* **2**, 033471 (2020).
- [28] When $V \ll \sqrt{g_n n_b}/M$, $Q \sim q - g_n M n_b V^2/q$, $\alpha^I \sim MV^2(g_n n_b - q)/(4q^2) - 1$, $\delta^I \sim V\sqrt{M}\sqrt{g_n n_b - q}/(\sqrt{2}q)$, $\beta^I \sim MV^2(q - g_n n_b)/(4q^2 + 1)$, and $\kappa^I \sim -V\sqrt{M}(g_n n_b - q)/(\sqrt{2}q)$.
- [29] Then, the components can be expressed as $K_{13}^I = \mathcal{K}^I \cos(\tau)$, $K_{23}^I = \mathcal{K}^I \sin(\tau)$, $K_{13}^{II} = -\mathcal{K}^{II} \cos(\tau)$, and $K_{23}^{II} = -\mathcal{K}^{II} \sin(\tau)$.
- [30] The other branch is $y \geq \sqrt{1 + \sqrt{1 - (q/g_n n_b)^2}}$, where $y = V/\sqrt{g_n n_b}/M$. However the condition $1 - y - \sqrt{y^2 + (q/g_n n_b)^2} - 2y > 0$ cannot be satisfied if $y > 1$. Hence this branch is not a solution. Other constraints $q - Q - MV^2 > 0$, $q + MV^2 - Q > 0$, and $q(Q - q) + g_n M n_b V^2 < 0$ can be reduced to $q - Q - MV^2 > 0$ which is always satisfied as long as $q/g_n n_b < 1$ and $MV^2/g_n n_b < q/g_n n_b$. Since $\sqrt{1 - \sqrt{1 - (q/g_n n_b)^2}} < q/g_n n_b$, these constraints are automatically satisfied.
- [31] L. Pitaevskii and S. Stringari, *Bose-Einstein Condensation and Superfluidity* (Oxford University Press, New York, 2016), Vol. 164.
- [32] See Supplemental Material at <http://link.aps.org/supplemental/10.1103/PhysRevLett.128.125301> for details and for a movie about the oscillating dynamics.
- [33] FDSs are the nontrivial extensions of the exact solutions found in Ref. [18] for finite V and are distinct from other known solvable cases in relevant multi-component systems [15,34]. Technically, a simple boost would not work to obtain traveling FDSs from the real wave functions of stationary MDWs at finite q . The wave functions of traveling FDSs are complex valued. Real and imaginary parts of each component of the wave function are nonlinearly coupled.
- [34] S. V. Manakov, *Sov. Phys. JETP* **38**, 248 (1974).
- [35] E. Yukawa and M. Ueda, *Phys. Rev. A* **86**, 063614 (2012).
- [36] Explicitly, they are $K_{13} = -2qN_{32}/\hbar$, $K_{23} = 2qN_{31}/\hbar$ and $K_{33} = 0$.
- [37] The total number current density is $\mathbf{J}_n = \sum_{m=-1,0,1} \mathbf{J}_m$.
- [38] A. Barone and G. Paterno, *Physics and Applications of the Josephson Effect* (Wiley, New York, 1982).
- [39] For $q = 0$, the Sine-Gordon representation of the magnetic domain wall allows nontrivial internal spin currents; however, they are not invariant under SO(3) spin rotations [18].
- [40] Since the density varies, the value of c_{FDS} also changes in space.
- [41] The linear potential should be chosen such that everywhere in the bulk is in the easy-plane phase, namely, $q < -2g_s \min[n(x)]$.
- [42] Here we adopt linear potentials to give a transparent illustration of the FDS dynamics. Transitions between the two types FDSs can take place in other situations when the maximum speed is reached.
- [43] The total (grand canonical) energy is $K_{\text{FDS}} + E_U$, where $E_U = \int dx nU$ is the potential energy and U is the external potential.
- [44] In a binary BEC, a bright-dark soliton with constant total density experiences oscillations when a weak force is imposed only on the bright soliton component [45]. Because the bright soliton sits in the density dip of the other (unaccelerated) component, and the density interaction between components causes the bright soliton to oscillate. The phenomenon and the mechanism are vastly different from what we discussed in this Letter.
- [45] L.-C. Zhao, W. Wang, Q. Tang, Z.-Y. Yang, W.-L. Yang, and J. Liu, *Phys. Rev. A* **101**, 043621 (2020).
- [46] M. Prüfer, P. Kunkel, H. Strobel, S. Lannig, D. Linnemann, C.-M. Schmied, J. Berges, T. Gasenzer, and M. K. Oberthaler, *Nature (London)* **563**, 217 (2018).
- [47] C.-M. Schmied, M. Prüfer, M. K. Oberthaler, and T. Gasenzer, *Phys. Rev. A* **99**, 033611 (2019).
- [48] L. Chomaz, L. Corman, T. Bienaimé, R. Desbuquois, C. Weitenberg, S. Nascimbène, J. Beugnon, and J. Dalibard, *Nat. Commun.* **6**, 6162 (2015).
- [49] G. Gauthier, I. Lenton, N. M. Parry, M. Baker, M. J. Davis, H. Rubinsztein-Dunlop, and T. W. Neely, *Optica* **3**, 1136 (2016).
- [50] G. Semeghini, G. Ferioli, L. Masi, C. Mazzinghi, L. Wolswijk, F. Minardi, M. Modugno, G. Modugno, M. Inguscio, and M. Fattori, *Phys. Rev. Lett.* **120**, 235301 (2018).
- [51] J. M. Higbie, L. E. Sadler, S. Inouye, A. P. Chikkatur, S. R. Leslie, K. L. Moore, V. Savalli, and D. M. Stamper-Kurn, *Phys. Rev. Lett.* **95**, 050401 (2005).
- [52] P. Kunkel, M. Prüfer, S. Lannig, R. Rosa-Medina, A. Bonnin, M. Gärtner, H. Strobel, and M. K. Oberthaler, *Phys. Rev. Lett.* **123**, 063603 (2019).